Electronic Nose Based on Multipatterns of ZnO Nanorods on a Quartz Resonator with Remote Electrodes

Wooree Ko, Namchul Jung, Moonchan Lee, Minhyuk Yun, and Sangmin Jeon*

Department of Chemical Engineering, Pohang University of Science and Technology (POSTECH), San 31, Hyoja-dong, Nam-gu, Pohang, Kyungbuk, Korea

ABSTRACT An electrodeless monolithic multichannel quartz crystal microbalance (MQCM) sensor was developed *via* the direct growth of ZnO nanorod patterns of various sizes onto an electrodeless quartz crystal plate. The patterned ZnO nanorods acted as independent resonators with different frequencies upon exposure to an electric field. The added mass of ZnO nanostructures was found to significantly enhance the quality factor (QF) of the resonator in electrodeless QCM configuration. The QF increased with the length of the ZnO nanorods; ZnO nanorods 5 μm in length yielded a 7-fold higher QF compared to the QF of a quartz plate without ZnO nanorods. In addition, the ZnO nanorods offered enhanced sensitivity due to the enlarged sensing area. The developed sensor was used as an electronic nose for detection of vapor mixtures with impurities.

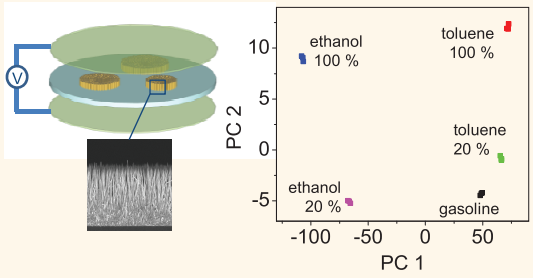

KEYWORDS: multichannel QCM · electrodeless QCM · ZnO nanostructures · quality factor · electronic nose

ZnO has attracted significant research interest for its unique properties and versatile applications in optics,[1] electronics,[2] photovoltaics,[3] and sensors.[4,5] Particularly, ZnO in nanostructure possesses a high surface-to-volume ratio,[6] excellent electromagnetic (EM) wave absorption property,[7] and tunable properties.[8] A variety of nanostructural forms have been developed including nanowires,[9] nanotubes,[10] nanotetrapods,[11] and nanorods,[12] using various synthetic mechanisms, and display unique chemical and physical properties. The large-scale synthesis of ZnO nanostructures can be easily realized at low cost, further contributing to its advantages and utility in practical applications.

ZnO nanostructures have been widely employed in sensors, such as field-effect transistor-type sensors and surface plasmon resonance and quartz crystal microbalance (QCM) sensors, for enhancement of efficiency and sensitivity.[13] Among these, a QCM is a label-free acoustic sensor used as a powerful tool for immunosensing,[14] DNA sensing,[15] and chemical sensing[16] owing to its high sensitivity and ease of measurement. The adsorption of analytes onto quartz crystals affects the effective mass of the quartz crystal, and the mass change is directly related to the change in the crystal resonance frequency as described by the Sauerbrey equation,[17]

$$\Delta f = -\frac{2{f_0}^2}{A\sqrt{\rho_q \mu_q}}\Delta m \qquad (1)$$

where f_0 is the resonance frequency of the unloaded crystal, Δm is the adsorbed mass, A is the active area of the quartz crystal between the deposited electrodes, ρ_q is the density of quartz (2.648 g/cm^3), and μ_q is the shear modulus of quartz (2.947 $\times$ 1011 g/cm/s^2). For simultaneous detection of multiple analytes without environmental influences or chip-to-chip variations that are inevitable with individual QCM sensors, a QCM with multiple resonators, that is, a monolithic multichannel QCM (MQCM),[18,19] has been developed. An MQCM is typically realized by fabricating multiple resonators with different resonance frequencies on a quartz plate, generally involving expensive and time-consuming micromachining processes. Also, the conventional MQCM faces problems associated with electrical lining, which becomes complicated, compact, and bulky when large numbers of resonators are involved.

* Address correspondence to jeons@postech.ac.kr.

Received for review March 7, 2013 and accepted July 24, 2013.

Published online July 24, 2013
10.1021/nn4027245

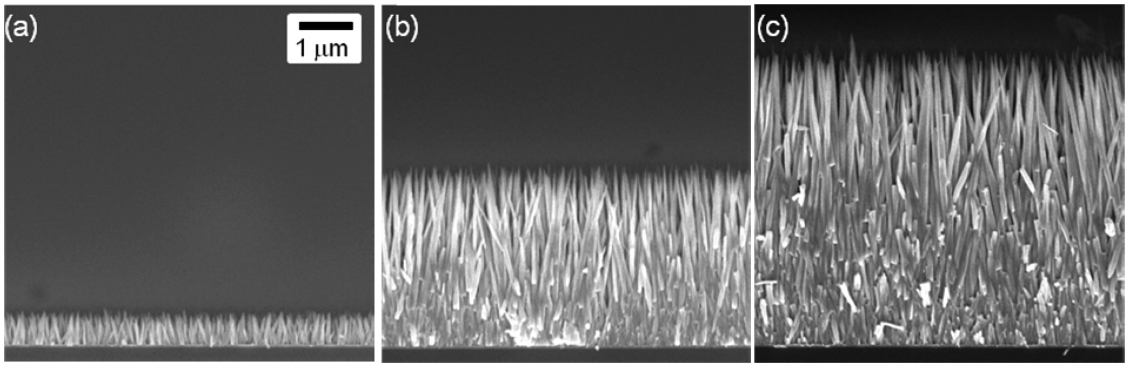

Figure 1. Side-view SEM images of ZnO nanorods grown on a silicon wafer for growth times of (a) 1 h, (b) 3 h, and (c) 5 h.

Here, we have developed an MQCM sensor using ZnO nanorods on an electrodeless quartz crystal plate. ZnO nanorods in differently sized patterns were synthesized directly onto a bare quartz crystal plate, and each pattern resulted in an independently functioning resonator in an electrodeless QCM, where the electrodes were physically separated and placed in close proximity to the surfaces of the quartz plate. An electrodeless QCM[20,21] generally displays a low QF due to the reduced transduction of electrical energy from the distant electrodes. However, we found that the employment of ZnO nanostructures not only enhanced the sensitivity through the enlarged sensing area but also significantly enhanced the QF of the electrodeless QCM. In addition, the adoption of an electrodeless QCM configuration significantly simplified the method to generate multiple resonators and to simultaneously measure the multiple resonance frequencies by requiring only a single pair of remote electrodes. The MQCM developed here was used as an electronic nose to detect the vapors of various mixed solutions.

RESULTS AND DISCUSSION

ZnO nanorods were grown directly on a 5 MHz bare quartz crystal plate (2.54 cm in diameter) using the hydrothermal method.[12] Figure 1a–c show scanning electron microscope (SEM) images of the ZnO nanorods. The average diameters (lengths) of the nanorods are 90 nm (0.7 μm), 100 nm (3.6 μm), and 130 nm (6.0 μm) at growth times of 1, 3, and 5 h, respectively. The ZnO nanorod-grown quartz plate was mounted in a sensing chamber with an integrated pair of 17 mm (diameter) circular electrodes. The distance between each electrode and the surface of the quartz plate was ca. 800 μm and was maintained by a pair of O-rings.

The QF-enhancing effect of the ZnO nanostructure in the electrodeless QCM was investigated by comparing the QFs of conventional and electrodeless quartz resonators before and after growing the ZnO nanorods in a 12 mm circular pattern. Figure 2a and b show the schematic representations of the experimental setups and conductance spectra of conventional and electrodeless QCMs with ZnO nanorods grown on each quartz resonator, respectively. The resonance peak of the bare quartz crystal in an electrodeless QCM configuration appeared at higher frequency than that in a conventional QCM configuration because of the absence of the gold coating. The QF of the resonators was calculated by dividing the resonance frequency by the full width at half-maximum of the peak. Figure 2c and d show the changes in resonance frequency and QF of conventional and electrodeless QCMs, respectively, as the length of the ZnO nanorods increases. The increasing length, that is, the increasing mass of ZnO nanorods, resulted in the decrease in the resonance frequencies of both the conventional and electrodeless QCMs as predicted by eq 1. However, the length of ZnO nanorods is shown to have a negligible effect on the QF of the conventional QCM, while it significantly increases that of the electrodeless QCM. The QF of the electrodeless QCM was initially lower than that of the conventional QCM due to the reduced transduction of electrical energy from the distant electrodes; however, the increasing length of the ZnO nanorods enhanced its QF, far exceeding the QF of the conventional QCM. The different effects of the ZnO nanostructures on the QF of each resonator are tentatively attributed to the position of the mass with respect to the position of the electrodes.

The synthesis of ZnO nanorods in patterns with various sizes can generate multiple resonators with different frequencies on an electrodeless quartz crystal plate. Figure 3a shows the top and side views of a quartz plate with two ZnO nanorod patterns (3 and 5 mm in diameter), and Figure 3b shows the conductance spectra of the quartz crystal at each growth hour. The SEM images of the ZnO nanorods at growth times of 2 h (1.9 μm) and 5 h (5.1 μm) are shown in the inset. At time 0 h, prior to ZnO nanorod growth, only one frequency, that is, the resonance frequency of the quartz plate, is measured. However, the growth of ZnO nanorods results in the appearance of two peak points at different frequencies, and the number of peak points corresponds to the number of ZnO nanorod patterns on the quartz plate. As the ZnO nanorods grow, each

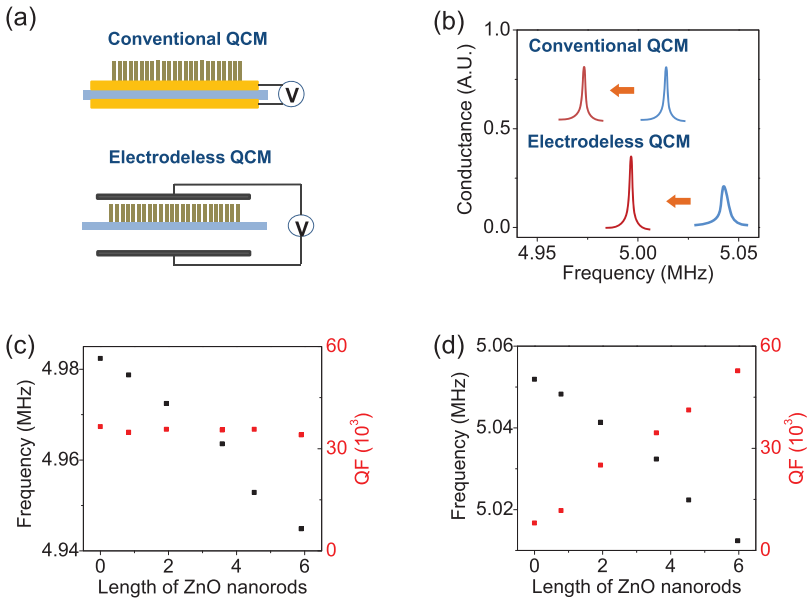

Figure 2. Schematic representations of electrode configurations (a) and conductance spectra (b) of conventional and electrodeless QCMs before (blue) and after (red) growing ZnO nanorods. Variations in frequency (black) and QF (red) of (c) a conventional QCM and (d) an electrodeless QCM as a function of ZnO nanorod length.

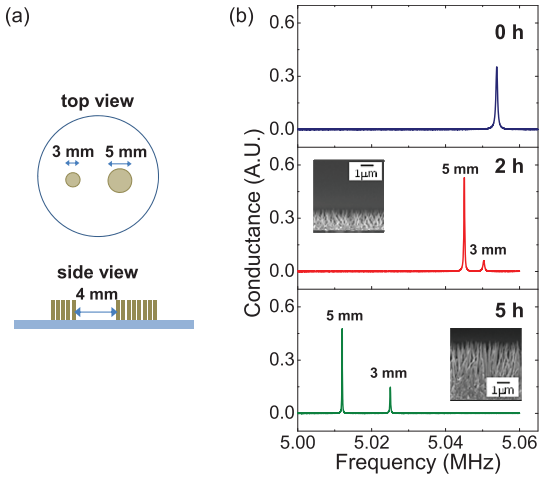

Figure 3. (a) Top and side views of a quartz plate with ZnO nanorod patterns of 3 and 5 mm in diameter. (b) Corresponding conductance spectra of the ZnO nanorod-patterned quartz crystal at growth times of 0, 2, and 5 h and the SEM images of the ZnO nanorods at growth times of 2 h (1.9 μm) and 5 h (5.1 μm).

pattern adds a different effective mass onto the quartz plate and causes different degrees of frequency changes. Each ZnO nanorod pattern functions as a resonator with a distinct frequency, and the frequency difference between two resonators increases with the length of the ZnO nanorods.

A higher number of resonators can be generated by increasing the number of ZnO nanorod patterns present. Figure 4a–c show the conductance spectra of quartz crystals prepared with two (QC2), three (QC3), or four (QC4) ZnO nanorod patterns, respectively, grown for 5 h. The pattern diameters were 3 and 5 mm for QC2; 3.5, 4.5, and 5.5 mm for QC3; and 3.5, 4.5, 5.5, and 6.5 mm for QC4. The number of distinct conductance peaks at different frequencies is equal to the number of ZnO nanorod patterns on each quartz crystal plate. This simple addition of patterned masses onto a bare quartz plate generates several distinct frequencies corresponding to their pattern sizes. Additional frequencies can be introduced by adjusting the pattern spacing, number, and size and, more critically, by using a thinner quartz plate. The rule of thumb for the minimum size of the ZnO pattern is 3 $\times$ (thickness of the quartz crystal), and the minimum distance between adjacent resonators is 7.5 $\times$ (thickness of the quartz crystal).[22] The thicknesses of 5 and 10 MHz quartz crystals are 300 and 150 μm, respectively. Note that the conductance increases as the size of the ZnO nanorod pattern increases because of the increase in the acoustic energy trapping.[23] For the simultaneous measurement of multiple frequencies, only a single pair of remote electrodes was used, rather than individual pairs of electrodes for each resonator. The electrodeless MQCM configuration greatly simplifies the design and operation of the instrument.

The active area of a QCM is important for determining its mass sensitivity. The active area of a ZnO nanorod-patterned electrodeless MQCM was determined by exposing a quartz plate with three ZnO nanorod patterns (Figure 5a) to 20% ethanol vapor. Figure 5b,c show the variations in the resonance frequencies of the three resonators divided by the square of the corresponding resonance frequency measured by exposure of the flat (Figure 5b) and ZnO nanorod-patterned (Figure 5c) sides of the quartz crystal plate to ethanol vapor for 300 s. The ZnO nanorod-patterned side yielded a 10-fold higher

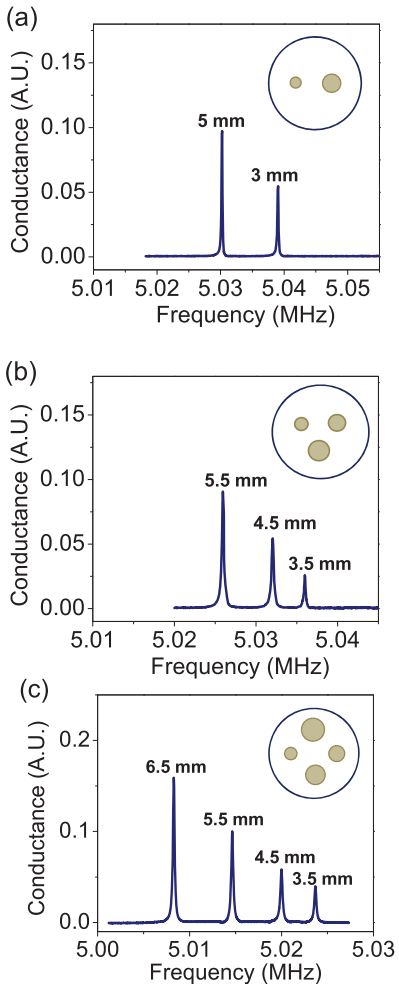

Figure 4. Conductance spectra of the quartz plates with (a) two patterns, (b) three patterns, and (c) four patterns of ZnO nanorods grown for 5 h.

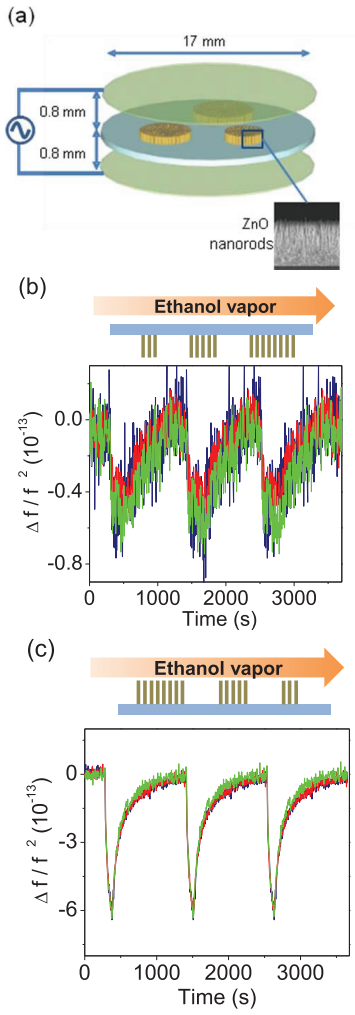

Figure 5. (a) Schematic illustration of electrodeless MQCM with three ZnO nanorod pattern (4, 5, and 6 mm in diameter). Normalized variations in the resonance frequencies of the electrodeless MQCM prepared with three resonators (blue, 6 mm; red, 5 mm; green, 4 mm) upon exposure of (b) the flat side or (c) the ZnO-NR side of the patterned quartz plate to 20% ethanol vapor.

frequency shift than the flat side of the MQCM due to the increased surface area, verifying the advantage of employing nanostructure for sensitivity enhancement. All three resonators showed reproducible and almost identical values of $\Delta f/f^2$ ($(6.27 \pm 0.05) \times 10^{-13}$ Hz^{-1}), which is, according to the Sauerbrey equation, proportional to $\Delta m/A$. The active area of the generated resonator, therefore, is solely confined to its own patterned area possibly because each ZnO nanorod pattern functions as a pseudoelectrode. As a result, the adsorption-induced frequency change does not depend on the size of each pattern.

The developed electrodeless MQCM was used as an electronic nose for the detection of vapor mixtures with impurities such as ethanol or toluene. A quartz plate prepared with three ZnO nanorod patterns (4, 5, and 6 mm in diameter) grown for 5 h was used, and each resonator was coated with 0.5% poly(methylmethacrylate) (PMMA), poly(vinylpyrrolidone) (PVP), or poly(vinyl acetate) (PVAc) by drop-casting. AFM images of the ZnO nanorods before and after the polymer coating showed negligible differences in the shape, indicating that the polymer coating produced a uniform thin film on the ZnO nanorods. Five samples, including the vapors of 100% gasoline (a mixture of hydrocarbons with various lengths), 100% toluene, 100% ethanol, and gasoline mixed with 20% (v/v) toluene or ethanol, were sequentially introduced into the sensing chamber for 30 s, followed by purging with nitrogen for 90 s. Note that ethanol and toluene are the typical adulterants of fake gasoline, which deteriorate the performance and emissions of automobile engines. Figure 6a–c show the variations of the resonance frequency of each resonator coated with PMMA, PVAc, or PVP, respectively, upon exposure to each vapor sample. The frequencies fully recovered to the original frequencies after purging, and the very similar responses of each resonator to three sequential sample flows of the same concentration show the high reproducibility of the MQCM response.

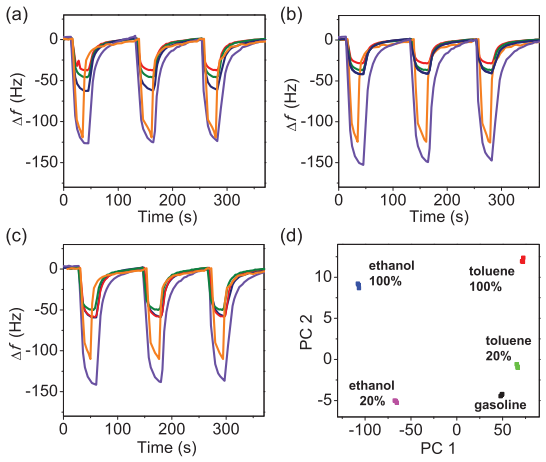

Figure 6. Variations in resonance frequencies of (a) PMMA-, (b) PVAc-, and (c) PVP-coated ZnO nanorod patterns upon exposure to 100% gasoline (blue), 100% toluene (red), gasoline with 20% (v/v) toluene (green), 100% ethanol (purple), and gasoline with 20% (v/v) ethanol (orange) and (d) PCA of the obtained frequency changes from (a), (b), and (c).

Figure 6d shows a principle component analysis (PCA) performed on the frequency data. Each vapor appears on a different position of the graph, indicating that the PCA can identify each sample. The PCA plot for the vapor mixtures with the impurities is expected to shift toward the upper left corner for the ethanol mixture and toward the upper right corner for the toluene mixture as the v/v % concentration of the impurity increases. The trajectories followed by the signal shifts are not expected to intersect. The electronic nose required only 2 min for rapid detection, another advantage of the electronic nose. The detection time can be further shortened by employing other coating layers that are more compatible with the adulterants.

CONCLUSION

In summary, we developed an electronic nose using a ZnO nanorod-patterned electrodeless MQCM. The patterned ZnO nanostructures resulted in the localized addition of mass that functioned as independent resonators with different frequencies. The growth of the ZnO nanostructures was found to significantly enhance the QF of the electrodeless QCM, thereby alleviating the major drawback to the electrodeless QCM. The ZnO nanostructure also contributed to the enhanced sensitivity of the sensor through the enlarged surface area. The multiple resonance frequencies were measured simultaneously by using only a single pair of electrodes, thereby solving the complicated instrumental problems associated with a conventional MQCM. The nanorod length and pattern size can be adjusted to further enhance the QF and sensitivity, as well as to introduce a larger number of resonators onto a single quartz plate. This MQCM has potential utility for drug screening or biosensing for the detection of multiple diseases.

METHODS

Materials. Zinc nitrate hexahydrate ($Zn(NO_3)_2 \cdot 6H_2O$, 98%), ammonium hydroxide (28 wt % NH_3 in water), PMMA, PVP, PVAc, and toluene (anhydrous, 99%), were purchased from Sigma-Aldrich (St. Louis, MO, USA). Ethanol was purchased from Merck. All chemicals were used as received. Toluene was used to prepare the PMMA and PVAc solutions. Deionized water (18.3 MΩcm) was obtained from a reverse osmosis water system (Human Science, Korea) and was used to prepare the PVP and $Zn(NO_3)_2 \cdot 6H_2O$ solutions. Gasoline was purchased from an S-Oil gasoline station (Korea).

Synthesis of ZnO Nanorods. Circular patterns of Ti (5 nm thick) and ZnO (30 nm thick) seed layers with different pattern diameters were sequentially sputtered onto one side of a 5 MHz quartz crystal. The sputtering conditions were set to a base pressure of 3×10^{-6} Torr and a working pressure of 7×10^{-3} Torr (Ar gas) with an RF power of 100 W at room temperature. ZnO nanorods were hydrothermally grown on the coated quartz crystal at 90 °C for various lengths of time in a 10 mM $Zn(NO3) \cdot 6H_2O$ solution at a pH of 10.6 by adding ammonia to the solution. The ZnO nanorod-grown quartz crystals were then rinsed with deionized water and ethanol prior to use.

Instrumental Setup. Circular electrodes of 17 mm were integrated into the chamber. The distance between each electrode and the surface of the quartz plate was approximately 0.8 mm. The pair of electrodes was connected to a custom-built PC-based conductance measurement system consisting of a function generator (NI PXI-5406), a digitizer (NI PXI-5114), and a multiplexer (NI PXI-2593) assembled in a PXI-1033 chassis (National Instruments, Austin, TX, USA). The measurement software was programmed in LabVIEW, and the conductance spectra were obtained by measuring the admittance and phase of a quartz crystal over the selected frequency span. The resonance frequencies of the ZnO nanorod patterns were evaluated based on Lorentzian fits of the conductance spectra, and changes in the resonant frequencies upon the adsorption of molecules were measured *in situ*. Gasoline with impurities was detected in a dry nitrogen carrier gas stream, which was bubbled through the gasoline sample with impurities to generate vapor. The gas flow was switched between the nitrogen stream and the vapor stream using three-way valves. The gas was introduced into the measurement chamber through two side inlets, and it exited through one central outlet. All the measurements were performed at room temperature and atmospheric pressure.

Principal Component Analysis. Principal component analysis is a mathematical procedure that simplifies data by reducing the number of dimensions. In this paper, PCS was conducted to convert a 3-D plot into a 2-D plot (Figure 6d). ZnO patterns coated with PMMA, PVAc, or PVP showed different frequency changes upon exposure to different analyte vapors. Each frequency change was then plotted on each *x*, *y*, and *z* axis.

i.e.,

$$\{(x, y, z) | x = \Delta f_{PMMA}, y = \Delta f_{PVAc}, z = \Delta f_{PVP}\}$$

In the same manner, a 3-D data set was obtained for various analytes. The obtained 3-D data set was then converted to a 2-D data set in the following steps:

(i) Adjust original data by subtracting a mean value from each dimension:

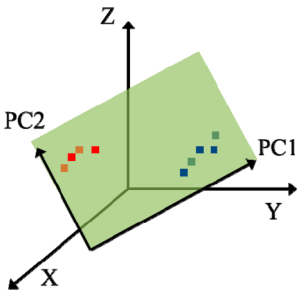

Data Adjust = $(x - y - z -)$, where the overbar indicates the mean of each dimension.

(ii) Make a 3 × 3 covariance matrix in which the components are the covariance (cov) between dimensions:

$$C = \begin{pmatrix} \mathrm{cov}(x,x) & \mathrm{cov}(x,y) & \mathrm{cov}(x,z) \\ \mathrm{cov}(y,x) & \mathrm{cov}(y,y) & \mathrm{cov}(y,z) \\ \mathrm{cov}(z,x) & \mathrm{cov}(z,y) & \mathrm{cov}(z,z) \end{pmatrix}$$

(iii) Obtain 3 eigenvectors for the covariance matrix, and also 3 corresponding eigenvalues.

(iv) Choose 2 eigenvectors by removing an eigenvector having the smallest eigenvalues.

(v) Make a feature vector in which the columns are the chosen eigenvectors:

$$\text{feature vector} = (\text{eigenvector 1} \quad \text{eigenvector 2})$$

$$= \begin{pmatrix} e_{i,1} & e_{i,2} \\ e_{j,1} & e_{j,2} \\ e_{k,1} & e_{k,2} \end{pmatrix}$$

(vi) Derive new 2-D data by multiplying the transpose of the data adjust (from (i)) with the transpose of the feature vector (from (v)):

$$\text{New 2-D data} = (\text{transposeof feature vector}) \times (\text{transpose of data adjust}) = \begin{pmatrix} x' \\ y' \end{pmatrix}$$

Conflict of Interest: The authors declare no competing financial interest.

Acknowledgment. This research was supported by Basic Science Research Program through the National Research Foundation of Korea (NRF) funded by the Ministry of Education (NRF-2011-0011246).

Supporting Information Available: Experimental setup, the conductance spectra of an electrodeless quartz crystal plate before and after growing ZnO nanorods, and AFM images of the ZnO nanorods before and after polymer coating. This material is available free of charge *via* the Internet at http://pubs.acs.org.

REFERENCES AND NOTES

1. Djurisic, A. B.; Leung, Y. H. Optical Properties of ZnO Nanostructures. *Small* **2006**, *2*, 944–961.
2. Nomura, K.; Ohta, H.; Ueda, K.; Kamiya, T.; Hirano, M.; Hosono, H. Thin Film Transistor Fabricated in Single-Crystalline Transparent Oxide Semiconductor. *Science* **2003**, *23*, 1269–1272.
3. Zhang, Q.; Dandeneau, C. S.; Zhou, X.; Cao, G. ZnO Nanostructures for Dye-Sensitized Solar Cells. *Adv. Mater.* **2009**, *21*, 4087–4108.
4. Zhao, Z.; Lei, W.; Zhang, X.; Wang, B.; Jiang, H. ZnO-Based Amperometric Enzyme Biosensors. *Sensors* **2010**, *10*, 1216–1231.
5. Joo, J.; Lee, D.; Yoo, M.; Jeon, S. ZnO Nanorod-Coated Quartz Crystals as Self-Cleaning Thiol Sensors for Natural Gas Fuel Cells. *Sens. Actuator B* **2009**, *138*, 485–490.
6. Lee, D.; Yoo, M.; Seo, H.; Tak, Y.; Kim, W. G.; Yong, K.; Lee, S. W.; Jeon, S. Enhanced Mass Sensitivity of ZnO Nanorod-Grown Quartz Crystal Microbalances. *Sens. Actuators B* **2009**, *135*, 444–448.
7. Chen, Y. J.; Cao, M. S.; Wang, T. H; Wan, Q. Microwave Absorption Properties of the ZnO Nanowire-Polyester Composites. *Appl. Phys. Lett.* **2004**, *84*, 3367–3369.
8. Hong, W. K.; Jo, G.; Sohn, J. I.; Park, W.; Choe, M.; Wang, G.; Kahng, Y. H.; Welland, M. E.; Lee, T. Tuning of the Electronic Characteristics of ZnO Nanowire Field Effect Transistors by Proton Irradiation. *ACS Nano* **2010**, *4*, 811–818.
9. Tsivion, D.; Schvartzman, M.; Popovitz-Biro, R.; Joselevich, E. Guided Growth of Horizontal ZnO Nanowires with Controlled Orientations on Flat and Faceted Sapphire Surfaces. *ACS Nano* **2012**, *6*, 6433–6445.
10. Li, Q. C.; Kumar, V.; Li, Y.; Zhang, H. T.; Marks, T. J.; Chang, R. P. H. Fabrication of ZnO Nanorods and Nanotubes in Aqueous Solutions. *Chem. Mater.* **2005**, *17*, 1001.
11. Yu, W. D.; Li, X. M.; Gao, X. D. Self-Catalytic Synthesis and Photoluminescence of ZnO Nanostructures on ZnO Nanocrystal Substrates. *Appl. Phys. Lett.* **2004**, *84*, 2658.
12. Tak, Y.; Yong, K. Controlled Growth of Well-Aligned ZnO Nanorod Array Using a Novel Solution Method. *J. Phys. Chem. B* **2005**, *109*, 19263–19269.
13. Djurisic, A. B.; Chen, X.; Leung, Y. H.; Ng, A. M. ZnO Nanostructures: Growth, Properties and Applications. *J. Mater. Chem.* **2012**, *22*, 6526.
14. Sakai, G.; Sakai, T.; Uda, T.; Miura, N.; Yamazoe, N. Evaluation of Binding of Human Serum Albumin (HSA) to Monoclonal and Polyclonal Antibody by Means of Piezoelectric Immunosensing Technique. *Sens. Actuators B* **1997**, *42*, 89–94.
15. Stengel, G.; Hook, F.; Knoll, W. Viscoelastic Modeling of Template-Directed DNA Synthesis. *Anal. Chem.* **2005**, *77*, 3709–3714.
16. Ozmen, A.; Tekce, F.; Ebeoglu, M. A.; Tasaltin, C.; Ozturk, Z. Z. Finding the Composition of Gas Mixtures by a Phthalocyanine-Coated QCM Sensors Array and an Artificial Neural Network. *Sens. Actuators B* **2006**, *115*, 450–454.
17. Sauerbrey, G. Z. Use of Quartz Crystal Vibrator for Weighting Thin Films on a Microbalance. *Z. Physik* **1959**, *155*, 206–222.
18. Tuantranont, A.; Wisitsora-at, A.; Sritongkham, P.; Jaruwongrungsee, K. A Review of Monolithic Multichannel Quartz Crystal Microbalance: A Review. *Anal. Chim. Acta* **2011**, *687*, 114–128.
19. Abe, T.; Esashi, M. One-Chip Multichannel Quartz Crystal Microbalance (QCM) Fabricated by Deep RIE. *Sens. Actuators A* **2000**, *82*, 139–143.
20. Larsson, E. M.; Edvardsson, E. M.; Langhammer, C.; Zoric, I.; Kasemo, B. A Combined Nanoplasmonic and Electrodeless Quartz Crystal Microbalance Setup. *Rev. Sci. Instrum.* **2009**, *80*, 125105.
21. Kunze, A.; Zach, M.; Svedhem, S.; Kasemo, B. Electrodeless QCM-D for Lipid Bilayer Applications. *Biosens. Bioelectron.* **2011**, *26*, 1833–1838.
22. Shen, F.; Lee, K. H.; O'Shea, S. J.; Lu, P.; Ng, T. Y. Frequency Interference between Two Quartz Crystal Microbalances. *IEEE Sens. J.* **2003**, *3*, 274–281.
23. Alekseev, S. G.; Mansfel'd, G. D.; Polzikova, N. I.; Kotelyanskii, I. M. Attenuation and Trapping of Acoustic Energy in Composite Mirocwave Resonators Based on YAG Single Crystals. *Acoust. Phys.* **2007**, *53*, 465–470.